

Article

Antiferromagnetic Oxide Thin Films for Spintronic Applications

Saima Afroz Siddiqui ¹, Deshun Hong ², John E. Pearson ²  and Axel Hoffmann ^{1,*} 

¹ Materials Research Laboratory, Department of Materials Science and Engineering, University of Illinois at Urbana Champaign, Urbana, IL 61801, USA; saimas@illinois.edu

² Materials Science Division, Argonne National Laboratory, Lemont, IL 60439, USA; dhong@anl.gov (D.H.); pearson@anl.gov (J.E.P.)

* Correspondence: axelh@illinois.edu

Abstract: Antiferromagnetic oxides have recently gained much attention because of the possibility to manipulate electrically and optically the Néel vectors in these materials. Their ultrafast spin dynamics, long spin diffusion length and immunity to large magnetic fields make them attractive candidates for spintronic applications. Additionally, there have been many studies on spin wave and magnon transport in single crystals of these oxides. However, the successful applications of the antiferromagnetic oxides will require similar spin transport properties in thin films. In this work, we systematically show the sputtering deposition method for two uniaxial antiferromagnetic oxides, namely Cr₂O₃ and α-Fe₂O₃, on A-plane sapphire substrates, and identify the optimized deposition conditions for epitaxial films with low surface roughness. We also confirm the antiferromagnetic properties of the thin films. The deposition method developed in this article will be important for studying the magnon transport in these epitaxial antiferromagnetic thin films.

Keywords: chromium oxide; hematite; reactive magnetron sputtering; epitaxial thin film; roughness; antiferromagnetic oxides



Citation: Siddiqui, S.A.; Hong, D.; Pearson, J.E.; Hoffmann, A. Antiferromagnetic Oxide Thin Films for Spintronic Applications. *Coatings* **2021**, *11*, 786. <https://doi.org/10.3390/coatings11070786>

Academic Editor: Paolo Mele

Received: 31 May 2021
Accepted: 24 June 2021
Published: 30 June 2021

Publisher's Note: MDPI stays neutral with regard to jurisdictional claims in published maps and institutional affiliations.



Copyright: © 2021 by the authors. Licensee MDPI, Basel, Switzerland. This article is an open access article distributed under the terms and conditions of the Creative Commons Attribution (CC BY) license (<https://creativecommons.org/licenses/by/4.0/>).

1. Introduction

Antiferromagnets have gained renewed interest due to their capability to support spin currents via their magnon excitations. This was first recognized in spin pumping experiments, where it was observed that spin currents can be conducted through much thicker insulating antiferromagnetic layers than conventional dielectric materials [1,2]. Subsequently, it was shown that the magnon contribution to heat currents in insulating antiferromagnets can give rise to spin Seebeck effects and therefore can be used to inject spin currents into adjacent metallic layers [3–5]. While this thermal spin current injection relied on incoherent magnons, it has in the meantime also been shown that spin current injection from coherently excited magnons is also possible [6,7]. More importantly, non-local transport measurements demonstrated the possibility to electrically inject and detect magnons in both Cr₂O₃ [8] and α-Fe₂O₃ [9,10]. Magnons can propagate over micrometer distances in both of these materials. Lastly, it has also been shown that current induced inhomogeneous temperature profiles can give rise to strains and thus allow to manipulate the magnetic structure within the insulating antiferromagnets [11]. Thus, antiferromagnetic insulators and specifically oxides are promising materials for spintronics applications (i.e., logic, memory, thermoelectric etc.) as they have zero resistive loss, tera-hertz spin dynamics and are immune to high magnetic fields [12,13]. In order to realize their full potential these applications require these antiferromagnetic materials in the thin film form [14].

In this article, we show the systematic variation of the thin films properties (film roughness and strain) of two antiferromagnetic hexagonal materials (i.e., Cr₂O₃ and α-Fe₂O₃ (Hematite)) by varying the deposition parameters (i.e., O₂ flow rate, deposition temperature and deposition pressure). There have been a few studies on the deposition of

these oxides in thin film form [15–17], in particular, on (0001) sapphire. We here show the epitaxial growth of these antiferromagnetic thin films on [11 $\bar{2}$ 0] sapphire substrates. These antiferromagnetic materials show no residual magnetism within the thickness ranging from 10 to 200 nm. However, the Morin transition was observed in α -Fe₂O₃ with thickness above 200 nm. The deposition process developed in this article will enable many exciting spintronic studies in these antiferromagnetic oxides.

2. Deposition Methods and Characterizations

In this work, we deposited Cr₂O₃ and α -Fe₂O₃ by using radio frequency (RF) magnetron sputtering at high temperature from 2'' Cr and Fe sputtering targets, respectively, on (11–20) Al₂O₃ (A-plane sapphire) substrates in the presence of both oxygen and argon. Initially, we varied the oxygen flow rate from 1.0 to 5.0 sccm while keeping the argon flow rate at 70 sccm and the chamber pressure at 3 mTorr. Here, we calibrated the deposition rate of Cr₂O₃ and the α -Fe₂O₃ using the crystal monitor. The temperature of the substrate was varied from 625 to 750 °C and the deposition pressure was varied from 2 to 5 mTorr for both Cr₂O₃ and α -Fe₂O₃.

The crystal orientation and the deposition rate of the epitaxial oxide films are characterized by X-ray diffraction (XRD) and X-ray reflectivity (XRR), respectively, using the Bruker D8 Advance XRD System (Bruker Corporation, Billerica, MA, USA) with a monochromatic Cu K α source with a wavelength of 1.54 Å. The roughness of the films is characterized by both XRR and atomic force microscopy (AFM) and the magnetic properties are characterized by superconducting quantum interference device (SQUID) magnetometer (Quantum Design North America, San Diego, CA, USA).

3. Results and Discussions

3.1. Crystal Structures of Epitaxial Oxide Films

Figure 1 shows the XRD data of the 20 nm Cr₂O₃ epitaxial films grown at 675 °C with an oxygen flow of 2.5 sccm and chamber pressure of 5 mTorr. The base pressure of the chamber was 3×10^{-8} Torr. After the deposition, the films were annealed at 700 °C for one hour at 2 mTorr in the presence of oxygen at 1 mTorr. XRD θ – 2θ patterns of film in Figure 1a show the peak at $2\theta = 36.02^\circ$, which comes from the Cr₂O₃ [11–20] Bragg reflection corresponding to the corundum structure. The peak at 37.8° is the [11–20] Al₂O₃ substrate peak. The films grown at oxygen flow varying from 2.0 to 3.5 sccm show similar structure with different strains in the films as discussed in detail below. It was, however, found that when the amount of O₂ in the gas mixture was above 5.0 sccm, the deposition rate decreased sharply. This finding is consistent with the previously reported results [18].

Figure 1b shows the rocking curve data for the [11–20] Bragg reflection of the same 20-nm Cr₂O₃ sample. The full width at half maximum value of the rocking curve is 0.145° . This indicates that the Cr₂O₃ film is formed with conformal a-axis orientation on the Al₂O₃ substrate. To confirm the epitaxial state of the in-plane orientation of the film, we performed the XRD Φ -scan of the Cr₂O₃ film from -190° to 190° (see Figure 1c). The Φ -scanning result from the Cr₂O₃ films indicates that there are two equivalent peaks, each being separated by 180° . These commensurate peak positions of the film and the substrate confirm the epitaxial relationship between the two. And this two-fold symmetry of the deposited film indicates that the film consists of a single crystalline domain.

We deposited both Cr₂O₃ and Fe₂O₃ samples by varying the flow rate of oxygen. The XRD θ – 2θ scan of the Cr₂O₃ thin films deposited with different oxygen flow are shown in Figure 2. The thickness of the films deposited at 3.5 sccm is 10 nm, while it is 20 nm for the other films deposited films. For both 2.5 and 3.0 sccm, the Cr₂O₃ peaks show finite size oscillations up to the fifth order, which confirms low surface roughness of these films. However, the film deposited with 3.5 sccm pressure shows a much broader XRD peak. The broadening may result from the shorter out of plane coherence length in thinner film [19]. Thus, for the subsequent depositions, we choose the oxygen flow of 2.5 sccm for

all the deposition conditions as this flow of oxygen provides the optimum oxidation for both oxides.

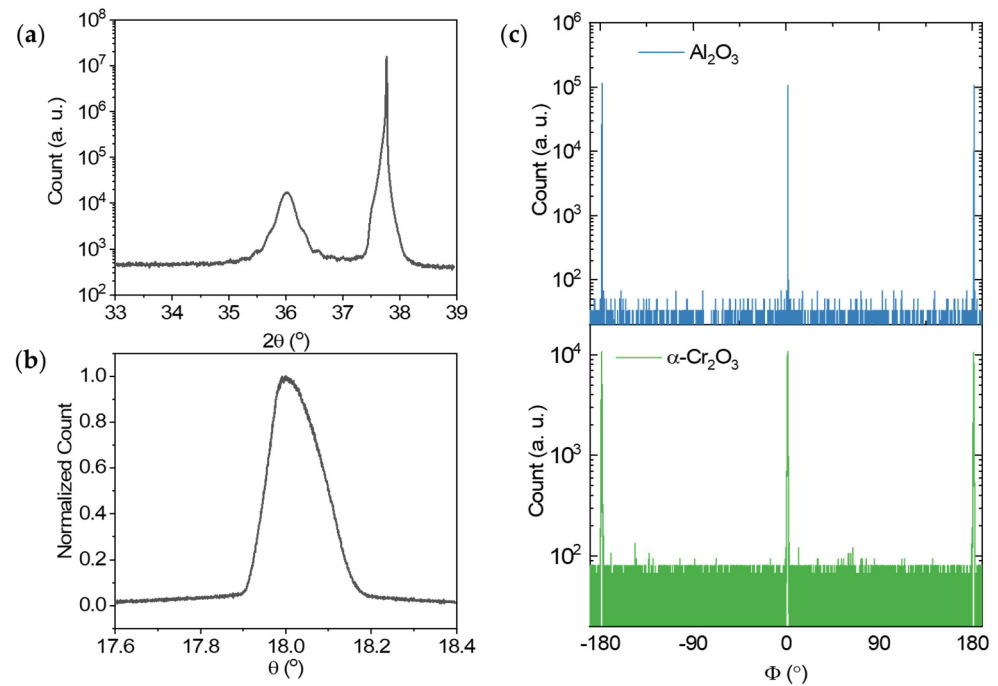


Figure 1. (a) XRD θ - 2θ patterns of the Cr_2O_3 epitaxial film grown on an $[11\bar{2}0]$ Al_2O_3 substrate. (b) XRD θ -rocking curve Cr_2O_3 film. (c) XRD Φ -scan results of the Cr_2O_3 and Al_2O_3 reflections.

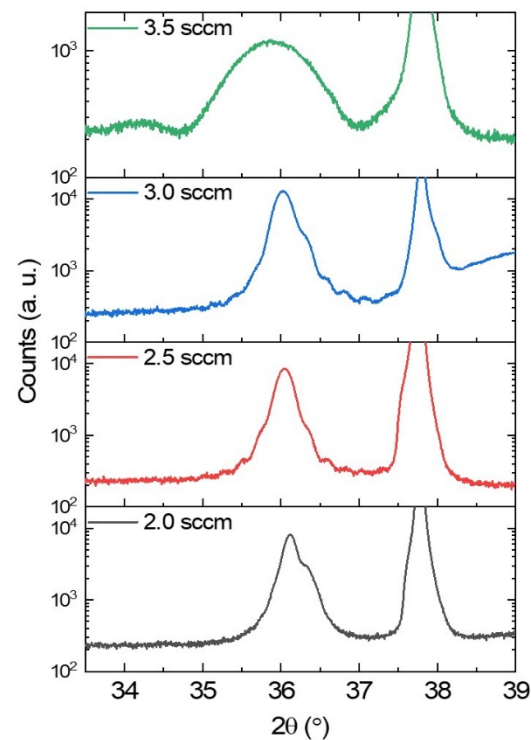


Figure 2. θ - 2θ scan of Cr_2O_3 thin films deposited with different oxygen flow at a deposition pressure of 5 mTorr and temperature of 675°C with 150 W RF power.

We characterize the roughness of the Cr_2O_3 epitaxial films using XRR. Figure 3a,b shows the roughness at different deposition temperatures as a function of O_2 flow and

deposition pressure, respectively. All the Cr_2O_3 films shown in Figure 3a were deposited with a chamber pressure of 5 mTorr. The roughness of the Cr_2O_3 films is lowest at the oxygen flow rate of 2.5 sccm and the deposition temperature of 675 °C. The roughness of the films increases for both lower and higher oxygen flow rate. Figure 3a also shows the in-plane compressive strain in Cr_2O_3 deposited at 675 °C due to lattice mismatch between the thin films and the sapphire substrate. Figure 3b shows that the roughness of the films gradually decreases for higher deposition pressure. We limit the deposition pressure to 5 mTorr to obtain an epitaxial film with low surface roughness while the deposition rate is still reasonable (3.5 Å/s). The low surface roughness of these antiferromagnet oxide films is important for the low damping of the magnon modes [20].

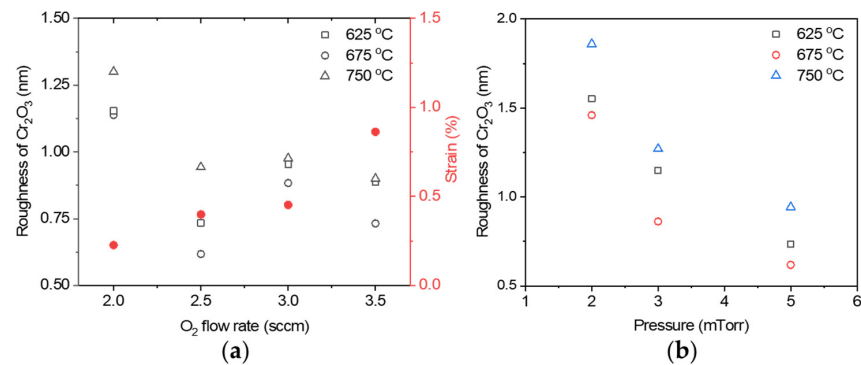


Figure 3. (a) Surface roughness of Cr_2O_3 films with thickness of 20 nm deposited at different temperature and in-plane compressive strain in Cr_2O_3 at 675 °C as a function of oxygen flow rate. The open symbols show the surface roughness, and the filled circles show the in-plane strain in Cr_2O_3 films. (b) Surface roughness of the films as a function of deposition pressure.

Figure 4 shows the XRD data of a 200-nm Fe_2O_3 film on an A-plane sapphire substrate. The peak at 35.6° is the $[11\bar{2}0]$ peak of $\alpha\text{-Fe}_2\text{O}_3$. This film is capped with 5 nm of Pt. The broader peak at 39.5° shows the $[111]$ XRD peak of the Pt layer. It was deposited on Fe_2O_3 at room temperature at a deposition pres \times 3 μm area and found to be only 3 Å (Figure 5). The in-plane Φ XRD-scan of the $\alpha\text{-Fe}_2\text{O}_3$ film indicates two-fold symmetry along the $\langle 11\bar{2}0 \rangle$ direction, and therefore, single crystalline domain structure. The roughnesses of thinner $\alpha\text{-Fe}_2\text{O}_3$ films show a similar trend with the oxygen flow and deposition pressure as observed for the Cr_2O_3 .

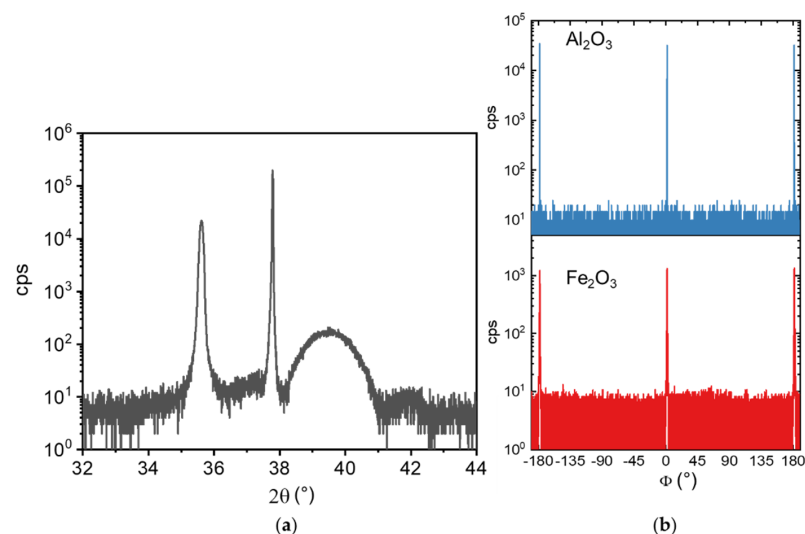


Figure 4. (a) XRD θ - 2θ patterns of the $\alpha\text{-Fe}_2\text{O}_3$ epitaxial film grown on an $[11\bar{2}0]$ Al_2O_3 substrate. (b) XRD Φ -scan results of the $\alpha\text{-Fe}_2\text{O}_3$ and Al_2O_3 reflections.

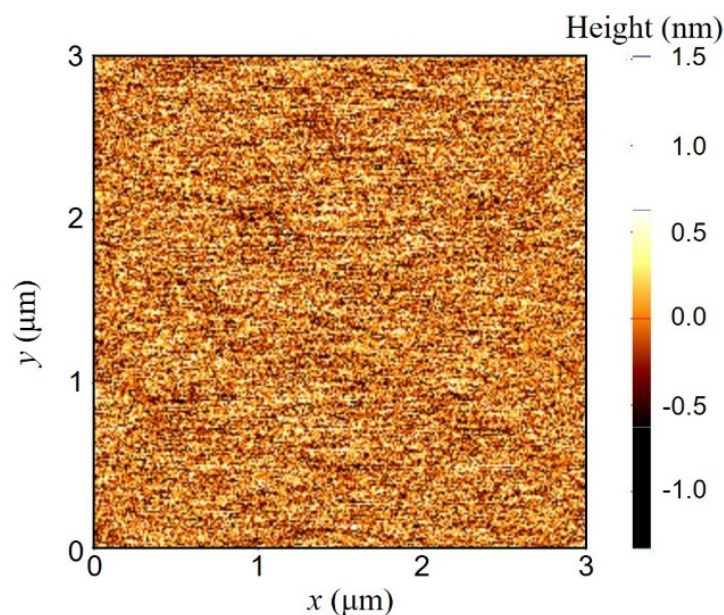


Figure 5. Atomic force micrograph of 200 nm thick α -Fe₂O₃ film.

3.2. Magnetic Properties

Cr₂O₃ and α -Fe₂O₃ are both antiferromagnetic materials. To confirm the absence of any residual magnetism in Cr₂O₃ and α -Fe₂O₃ films, SQUID measurements were performed with magnetic fields of 0.4 and 0.2 T, respectively, applied perpendicular to the A-plane of the substrates. For the SQUID measurement, a 5 × 5 mm sample is loaded in the chamber inside a straw. The sample plane is perpendicular to the magnetic field. Figure 6 shows the magnetization of the epitaxial oxide films as a function of temperature. There is no hysteresis present in the magnetization data between the heating and cooling of the Cr₂O₃ films from 5 to 320 K and, of the α -Fe₂O₃ films from 5 to 350 K. For the 20-nm Cr₂O₃ films, the magnetization is almost zero, which identifies the antiferromagnetic exchange interaction between Cr³⁺ ions in neighboring layers [21]. There is no significant difference observed between the zero-field cooled (ZFC) and the field cooled (FC) measurements. For the FC measurement, the sample is cooled to 5 K from 320 K with a magnetic field of 2 T applied perpendicular to the A-plane of the substrate. We noticed a very small (0.01 emu/cm³) increase in the magnetization at 40 K for 20-nm Cr₂O₃ epitaxial films. This minuscule magnetization comes from the magnetic impurities present in the sapphire substrates as confirmed by measuring the magnetization of only the substrate as a function of temperature (data not presented). The inset of Figure 6a shows the spin orientation of the Cr³⁺ ions inside a unit cell of Cr₂O₃. The spins are pointing along the c-axis of the sample for all temperatures.

In α -Fe₂O₃, the antiferromagnetic spin configuration changes its direction from being parallel to the [0001] axis to being in the (0001) basal plane at temperatures above the Morin temperature (T_M). The Morin transition is due to the Dzyaloshinskii–Moriya interaction, where asymmetric exchange interaction between two neighboring spins results in a weak net magnetic moment in the (0001) plane at temperatures above T_M [22]. Figure 4b shows the temperature dependence of the out-of-plane magnetization of a 200-nm thick α -Fe₂O₃ film under an applied field of 0.2 T. An increase of the magnetization is observed above 225 K, which is lower than in bulk samples (\approx 260 K) [22]. The enhanced magnetization reflects a weak net ferromagnetic moment at temperatures above T_M . For thinner α -Fe₂O₃ samples, we did not observe the Morin transition. The lowering of the transition temperature in thinner films may result from the increased in-plane strain in those films. The Morin transition is usually determined by the competition between the magnetic dipolar and the structural anisotropy energies. The temperature variations of these two energy contributions have quantum statistical basis and are different [23]. It is possible that

their temperature variations change compared to bulk crystals because of the presence of strain in the film, which eventually eliminates the secondary transition.

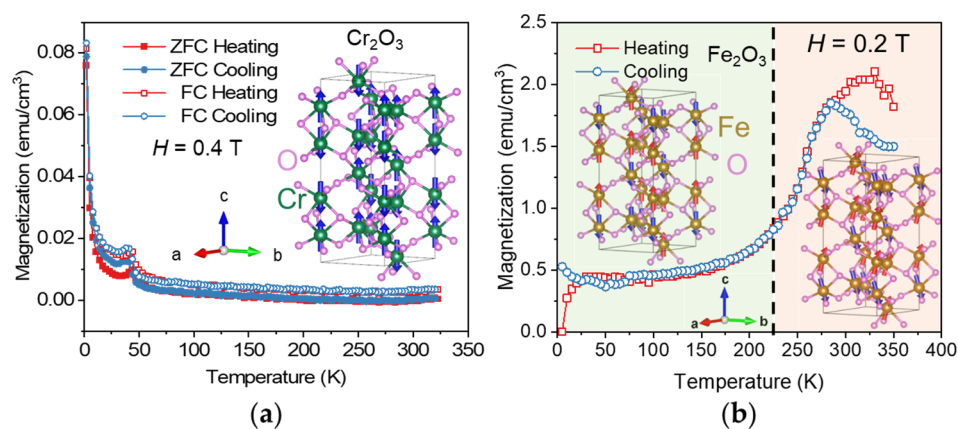


Figure 6. Magnetization of (a) Cr_2O_3 , (b) $\alpha\text{-Fe}_2\text{O}_3$ epitaxial films along the a-axis as a function of temperature. A magnetic field of 2 T is applied perpendicular to the A-plane during the field-cooling for the Cr_2O_3 film. The inset of (a) shows the unit cell of Cr_2O_3 with the spin orientations for the Cr^{3+} ions. The insets of (b) show the unit cells of $\alpha\text{-Fe}_2\text{O}_3$ with the spin orientations for the Fe^{3+} ions before and after the Morin transition.

4. Conclusions

In summary, we have shown a detailed study of radio frequency magnetron sputtering of epitaxial thin films of Cr_2O_3 and $\alpha\text{-Fe}_2\text{O}_3$ on A-plane sapphire substrates for spintronic applications. Optimized sputtering conditions are discussed together with the characterizations of the crystal orientations and magnetic properties of these films. These single domain antiferromagnetic oxide thin films will be very important for studying the magnon dynamics and transport for extremely low-loss spintronic devices. They can also potentially be used for antiferromagnetic ultra-dense memory with THz bandwidth by utilizing current induced magnetization reversal. In addition, our developed deposition method confirms the single domain properties of these films, which is essential to reproduce many exciting magnon properties, which were previously observed only in single crystal oxides. Our epitaxial sputtering method will pave the way for the potential application of antiferromagnetic oxides in the field of electronics.

Author Contributions: S.A.S. conceived, designed and performed the experiments, and analyzed the data. D.H. helped with the $\alpha\text{-Fe}_2\text{O}_3$ structural characterization. J.E.P. helped with the deposition and characterization of the $\alpha\text{-Fe}_2\text{O}_3$ films. S.A.S. and A.H. co-wrote the paper. All authors have read and agreed to the published version of the manuscript.

Funding: The growth and the characterization of $\alpha\text{-Fe}_2\text{O}_3$ films were supported by the US Department of Energy, Office of Science, Basic Energy Sciences, Materials Sciences and Engineering Division. The use of facilities at the Center for Nanoscale Materials, an Office of Science user facility, was supported by the US Department of Energy, Basic Energy Sciences under Contract No. DE-AC02-06CH11357. The growth and the characterization of Cr_2O_3 films were supported by the National Science Foundation (NSF) through the University of Illinois at Urbana-Champaign Materials Research Science and Engineering Center No. DMR-1720633 and was carried out in part in the Materials Research Laboratory Central Research Facilities, University of Illinois.

Institutional Review Board Statement: Not applicable.

Informed Consent Statement: Not applicable.

Data Availability Statement: The data presented in this study are available on request from the corresponding author.

Conflicts of Interest: The authors declare no conflict of interest. The funders had no role in the design of the study; in the collection, analyses, or interpretation of data; in the writing of the manuscript, or in the decision to publish the results.

References

1. Wang, H.; Du, C.; Hammel, P.C.; Yang, F. Antiferromagnonic spin transport from $\text{Y}_3\text{Fe}_5\text{O}_{12}$ into NiO. *Phys. Rev. Lett.* **2014**, *113*, 097202. [[CrossRef](#)]
2. Hahn, C.; de Loubens, G.; Naletov, V.V.; Ben Youssef, J.; Klein, O.; Viret, M. Conduction of spin currents through insulating antiferromagnetic oxides. *EPL Europhys. Lett.* **2014**, *108*, 57005. [[CrossRef](#)]
3. Seki, S.; Ideue, T.; Kubota, M.; Kozuka, Y.; Takagi, R.; Nakamura, M.; Kaneko, Y.; Kawasaki, M.; Tokura, Y. Thermal generation of spin current in an antiferromagnet. *Phys. Rev. Lett.* **2015**, *115*, 266601. [[CrossRef](#)]
4. Wu, S.M.; Zhang, W.; Kc, A.; Borisov, P.; Pearson, J.E.; Jiang, J.S.; Lederman, D.; Hoffmann, A.; Bhattacharya, A. Antiferromagnetic spin seebeck effect. *Phys. Rev. Lett.* **2016**, *116*, 097204. [[CrossRef](#)]
5. Luo, Y.; Liu, C.; Saglam, H.; Li, Y.; Zhang, W.; Zhang, S.S.; Pearson, J.E.; Fisher, B.; Zhou, T.; Bhattacharya, A.; et al. Distinguishing antiferromagnetic spin sublattices via the spin Seebeck effect. *Phys. Rev. B* **2021**, *103*, L020401. [[CrossRef](#)]
6. Li, J.; Wilson, C.B.; Cheng, R.; Lohmann, M.; Kavand, M.; Yuan, W.; Aldosary, M.; Agladze, N.; Wei, P.; Sherwin, M.S.; et al. Spin current from sub-terahertz-generated antiferromagnetic magnons. *Nature* **2020**, *578*, 70–74. [[CrossRef](#)]
7. Vaidya, P.; Morley, S.A.; van Tol, J.; Liu, Y.; Cheng, R.; Brataas, A.; Lederman, D.; del Barco, E. Subterahertz spin pumping from an insulating antiferromagnet. *Science* **2020**, *368*, 160. [[CrossRef](#)]
8. Yuan, W.; Zhu, Q.; Su, T.; Yao, Y.; Xing, W.; Chen, Y.; Ma, Y.; Lin, X.; Shi, J.; Shindou, R.; et al. Experimental signatures of spin superfluid ground state in canted antiferromagnet Cr_2O_3 via nonlocal spin transport. *Sci. Adv.* **2018**, *4*, eaat1098. [[CrossRef](#)]
9. Lebrun, R.; Ross, A.; Bender, S.A.; Qaiumzadeh, A.; Baldrati, L.; Cramer, J.; Brataas, A.; Duine, R.A.; Kläui, M. Tunable long-distance spin transport in a crystalline antiferromagnetic iron oxide. *Nature* **2018**, *561*, 222–225. [[CrossRef](#)]
10. Lebrun, R.; Ross, A.; Gomonay, O.; Baltz, V.; Ebels, U.; Barra, A.L.; Qaiumzadeh, A.; Brataas, A.; Sinova, J.; Klau, M. Long-distance spin-transport across the Morin phase transition up to room temperature in ultra-low damping single crystals of the antiferromagnet $\alpha\text{-Fe}_2\text{O}_3$. *Nat. Commun.* **2020**, *11*, 6332. [[CrossRef](#)]
11. Zhang, P.; Finley, J.; Safi, T.; Liu, L. Quantitative study on current-induced effect in an antiferromagnet insulator/Pt bilayer film. *Phys. Rev. Lett.* **2019**, *123*, 247206. [[CrossRef](#)]
12. Kosub, T.; Kopte, M.; Hühne, R.; Appel, P.; Shields, B.; Maletinsky, P.; Hübner, R.; Liedke, M.O.; Fassbender, J.; Schmidt, O.G.; et al. Purely antiferromagnetic magnetoelectric random access memory. *Nat. Commun.* **2017**, *8*, 13985. [[CrossRef](#)]
13. Ramazanov, S.; Sobola, D.; Orudzhev, F.; Knápek, A.; Polčák, J.; Potoček, M.; Kaspar, P.; Dallaev, R. Surface modification and enhancement of ferromagnetism in BiFeO_3 nanofilms deposited on HOPG. *Nanomaterials* **2020**, *10*, 1990. [[CrossRef](#)] [[PubMed](#)]
14. Speriosu, V.S.; Herman, D.A.; Sanders, I.L.; Yogi, T. Magnetic thin films in recording technology. *IBM J. Res. Dev.* **1990**, *34*, 884–902. [[CrossRef](#)]
15. Leighton, C.; Hoffmann, A.; Fitzsimmons, M.R.; Nogués, J.; Schuller, I.K. Deposition of epitaxial $\alpha\text{-Fe}_2\text{O}_3$ layers for exchange bias studies by reactive dc magnetron sputtering. *Philos. Mag. B* **2001**, *81*, 1927–1934. [[CrossRef](#)]
16. Valeri, S.; Altieri, S.; Luches, P. Growth of antiferromagnetic oxide thin films. *Magn. Prop. Antiferromagn. Oxide Mater.* **2010**, 25–68. [[CrossRef](#)]
17. Shimomura, N.; Pati, S.P.; Sato, Y.; Nozaki, T.; Shibata, T.; Mibu, K.; Sahashi, M. Morin transition temperature in (0001)-oriented $\alpha\text{-Fe}_2\text{O}_3$ thin film and effect of Ir doping. *J. Appl. Phys.* **2015**, *117*, 17C736. [[CrossRef](#)]
18. Rothhaar, U.; Oechsner, H. Rf magnetron sputter deposition of Cr_2O_3 layers on ceramic Al_2O_3 substrates. *Surf. Coat. Technol.* **1993**, *59*, 183–186. [[CrossRef](#)]
19. Vayunandana Reddy, Y.K.; Wolfman, J.; Autret-Lambert, C.; Gervais, M.; Gervais, F. Strain relaxation of epitaxial $(\text{Ba}_{0.6}\text{Sr}_{0.4})(\text{Zr}_{0.3}\text{Ti}_{0.7})\text{O}_3$ thin films grown on SrTiO_3 substrates by pulsed laser deposition. *J. Appl. Phys.* **2010**, *107*, 106101.
20. Yu, T.; Sharma, S.; Blanter, Y.M.; Bauer, G.E. Surface dynamics of rough magnetic films. *Phys. Rev. B* **2019**, *99*, 174402. [[CrossRef](#)]
21. Nozaki, T.; Al-Mahdawi, M.; Shiokawa, Y.; Pati, S.P.; Imamura, H.; Sahashi, M. Magnetic anisotropy of doped Cr_2O_3 antiferromagnetic films evaluated by utilizing parasitic magnetization. *J. Appl. Phys.* **2020**, *128*, 023901. [[CrossRef](#)]
22. Morin, F.J. Electrical properties of $\alpha\text{-Fe}_2\text{O}_3$ and $\alpha\text{-Fe}_2\text{O}_3$ containing titanium. *Phys. Rev.* **1951**, *83*, 1005–1010. [[CrossRef](#)]
23. Artman, J.O.; Murphy, J.C.; Foner, S. Magnetic anisotropy in antiferromagnetic corundum-type sesquioxides. *Phys. Rev.* **1965**, *138*, A912–A917. [[CrossRef](#)]